A GLOBALLY CONVERGENT ALGORITHM FOR THE FREQUENCY SOUNDING AND SLICHTER-LANGER-TIKHONOV PROBLEM OF ELECTRICAL PROSPECTING *

MICHAEL V. KLIBANOV† AND ALEXANDRE TIMONOV‡

Abstract. The paper presents a globally convergent algorithm for solving coefficient inverse problems. Being rooted in the globally convergent numerical method (SIAM J. Sci. Comput., **31**, No.1 (2008), pp. 478-509) for solving multidimensional coefficient inverse problems, it has two distinctive features: the new iterative and refinement procedures. These novelties enhance, sometimes significantly, both the spatial and contrast resolutions. The computational effectiveness of the proposed technique is demonstrated in numerical experiments with two applied coefficient inverse problems: electromagnetic or acoustic frequency sounding and electrical prospecting of layered media. The Slichter-Langer-Tikhonov formulation is exploited as a mathematical model of the latter.

Key words. Coefficient inverse problem, globally convergent algorithm, boundary and internal data

AMS subject classifications. 15A15, 15A09

1. Introduction. The paper addresses a challenging problem of constructing globally convergent algorithms for Coefficient Inverse Problems (CIPs), i.e., the inverse problems for the partial differential equations where one needs to determine one or several coefficients from a given solution (or its functionals) on some manifolds (see, e.g., [3], [7], [15] and references cited there). In this paper, the global convergence is understood in the sense that a reconstruction algorithm produces a sequence of iterates that converge to the sought coefficient or to its "good" estimate from an initial approximation, which is not necessarily close to this coefficient.

Due to both the nonlinearity and ill-posedness of CIPs, providing the global convergence is important for many, if not for all, reconstruction algorithms. Being applied to a CIP, the nonlinear least squares approach normally results in a nonconvex minimization problem. Clearly, under such conditions, the traditional numerical techniques, such as the gradient or Newton-like methods, may be not applicable or they may fail to converge to the true solution. On the other hand, the methods of global optimization are extremely time consuming and heuristic. Thus, the development of globally convergent algorithms is of particular interest to quantitative imaging in defence science, geophysics, medical diagnostics, non-destructive testing and evaluation, etc.

The goal of this paper is twofold. First, this is to present a globally convergent algorithm for solving some CIPs in one dimension. Second, this is to demonstrate its computational effectiveness by applying it to frequency sounding and resistivity prospecting of layered media. Introduced by Tikhonov [26] and Cagniard [4] in exploration geophysics, the method of frequency sounding became one of the most popular techniques used in a variety of applications (see, e.g., survey [9]). The term "resistivity prospecting" is associated with geophysical prospecting techniques utilizing measurements of the voltage potential produced by currents injected from the Earth's surface

*Received by the editors February, 2013; accepted for publication, ; published electronically .

†Department of Mathematics and Statistics, University of North Carolina at Charlotte, Charlotte, NC, USA (mklibanv@math.uncc.edu).

‡Division of Mathematics and Computer Science, University of South Carolina Upstate, Spartanburg, SC, USA (atimonov@uscupstate.edu).

into the ground (see, e.g. [30]). Unlike the Calderon formulation which is widely used in electrical impedance tomography with multiple boundary measurements, we utilize the Slichter-Langer-Tikhonov mathematical model [13], [20], [27] with a single boundary measurement. Based, in general, on three dimensional mathematical models, these CIPs allow, nevertheless, for one dimensional formulations making, by the same token, more descriptive the underlying ideas of the proposed algorithm. On the other hand, one dimensional quantitative imaging is widely used in many applications, such as studying Earth interior [21] and seafloor resources [6], as well as in studying macromolecular biological interactions [22], nuclear magnetic resonance 1D imaging [16], mine countermeasures [12], etc.

The globally convergent numerical method for solving the hyperbolic CIPs was proposed and developed in [2], [3], [7], [10], [11], [12]. In [7] the authors utilized the Carleman estimates and constructed some strictly convex least squares functionals at each step of a layer stripping procedure with respect to the spatial variable. In [2], [3], [10], [11], [12] the layer stripping procedure with respect to the real-valued parameter of the Laplace transform combined with an iterative procedure for treatment of the so-called tails was developed and applied to solving nD ($n = 1, 2, 3$) CIPs. Being rooted in the globally convergent numerical method [2], the proposed algorithm possesses two new features. First, in the iterative procedure for solving an overdetermined boundary value problem for the nonlinear second-order differential equation the successive approximations are constructed for every parameter from the Laplace transform. Second, we refine the iterative solution by matching the interior field generated by this solution with the solution of the forward problem in the region of interest unlike the traditional refinement by matching the boundary data. This technique differs significantly from a refinement procedure (see [3]) based on the adaptive FM/FD methods [1].

The paper is formatted as follows. In the next section, a generic coefficient inverse problem is formulated to exemplify our approach. In section 3 we describe the proposed algorithm. In sections 4 and 5 we state convergence results for both the successive approximations produced by the proposed algorithm and their refinements. In section 6 we conduct the numerical study to demonstrate the computational effectiveness of the proposed algorithm. We conclude our investigation in section 7.

2. Problem formulation. We introduce a generic coefficient inverse problem as follows. Let $\Omega \subset R^3$ be a convex bounded domain with a sufficiently smooth boundary $\partial\Omega$. Let the function $\mu(x) \geq 1$ be such that $\mu \in C^2(R^3), \mu(x) = 1$ for $x \in R^3 \backslash \Omega$. Consider the Cauchy problem for the hyperbolic equation

$$\mu(x) U_{tt} - \Delta U = 0 \quad \text{in } R^3 \times (0, \infty), \tag{2.1}$$

$$U(x, 0) = 0, \quad U_t(x, 0) = \delta(x - x_0). \tag{2.2}$$

In particular, if the problem (2.1)-(2.2) models the propagation and scattering of the electromagnetic or acoustic field, then $\mu(x) = c^{-2}(x)$, where $c(x)$ is the speed of electromagnetic or acoustic waves. We emphasize that we do not impose the smallness assumption on the coefficient μ.

Generic Coefficient Inverse Problem (GCIP). *Let the function $U(x, t)$ be the solution of the Cauchy problem (2.1)-(2.2). Given a single measurement $U(x, t) = f(x, t)$ on the boundary $\partial\Omega$ for a fixed source position $x_0 \notin \overline{\Omega}$ and for all $t \in (0, \infty)$, find the coefficient $\mu(x)$ in Ω.*

To our knowledge, there is no global uniqueness result for the GCIP available in the mathematics literature. We assume below uniqueness of the solution of GCIP,

because we will utilize the generic inverse problem only for the purpose of describing the globally convergent algorithm. Consider the Laplace transform of the function $U(x,t)$ for $s \geq \underline{s}$, where $\underline{s}$ is a positive constant,

$$u(x,s) = \int_0^\infty U(x,t)e^{-st}dt, \quad s \geq \underline{s} = const. > 0.$$

It follows from [3] (see Theorem 2.7.1) that for all $s \geq \underline{s}$, where $\underline{s}$ is sufficiently large, the function $u(x,s)$ is the unique solution of the problem

$$\Delta u - s^2\mu(x)u = -\delta(x - x_0), \quad x \in R^3, \tag{2.3}$$

$$\lim_{|x|\to\infty} u(x,s) = 0 \tag{2.4}$$

satisfying the following conditions

$$u(x,s) > 0, \forall x \neq x_0; u(x,s) = \frac{\exp(-s|x-x_0|)}{4\pi|x-x_0|} + \overline{u}(x,s), \overline{u} \in C^{2+\alpha}\left(R^3\right) \tag{2.5}$$

for all $\alpha \in (0,1)$. Furthermore, for any $s > 0$ the theorem 2.7.2 in [3] ensures existence of a unique solution of the problem (2.3), (2.4) satisfying conditions 2.5). In this paper, $C^{k+\alpha}$ are Hölder spaces, where $k \geq 0$ is an integer and $\alpha \in (0,1)$.

For simplicity, we describe the proposed algorithm in one dimension. Its generalization to two and three dimensions is straightforward. In one dimension, $\Omega = (0,1)$, and the source is located outside of this interval, i.e., $x_0 \in \{x < 0\}$. Also, we assume that the function $\mu(x)$ satisfies the following conditions

$$\mu \in C^\alpha(R), \mu(x) \in [1,m], \mu(x) = 1 \text{ for } x \notin (0,1), \tag{2.6}$$

where the number $m > 1$ is given. Then a single measurement is given by $U(0,t) = f(t)$, and the one dimensional analogue of the problem (2.3)-(2.4) acquires the form

$$u_{xx} - s^2\mu(x)u = -\delta(x - x_0), \quad x \in R, \tag{2.7}$$

$$\lim_{|x|\to\infty} u(x,s) = 0. \tag{2.8}$$

It follows from [12] (see the theorem 3.1) that the Laplace transform of $U(x,t)$ satisfies the problem (2.7)-(2.8) for all $s \geq \underline{s}$ for a sufficiently large $\underline{s} > 0$, and for all $s > 0$ there exists a unique solution $u(x,s)$ of the problem (2.7), (2.8). It satisfies the analogue of (2.5)

$$u(x,s) > 0, \forall x \in R; u(x,s) = u_0(x,s) + \overline{u}(x,s), \overline{u} \in C^{2+\alpha}(R), \tag{2.9}$$

where

$$u_0(x,s) = \frac{\exp(-s|x-x_0|)}{2s}$$

is the solution of the problem (2.7)-(2.8) with $\mu(x) \equiv 1$. Let $\varphi(s)$ be the Laplace transform of $f(t)$. Since $\mu(x) = 1$ for $x < 0$, then given $\varphi(s)$, one can uniquely determine the function $u_x(0,s) = s\varphi(s) - \exp(sx_0) := \tilde{\varphi}(s)$ (see, e.g., [12]).

Now we introduce a new function

$$v(x,s) = \frac{1}{s^2}\ln\left(\frac{u}{u_0}\right). \tag{2.10}$$

Then the problem (2.7)-(2.8) is reduced to the problem

$$v_{xx} + s^2 v_x^2 - 2sv_x = \mu(x) - 1 \quad \text{in } (0,1), \tag{2.11}$$

$$v(0,s) = v_0(s), \quad v_x(0,s) = v_1(s), \tag{2.12}$$

where

$$v_0(s) = \frac{\ln \varphi(s) - \ln 2s}{s^2} + \frac{x_0}{s}, v_1(s) = \frac{2}{s} - \frac{e^{sx_0}}{s^2 \varphi(s)}.$$

Introducing one more function $q(x,s) = \partial_s v(x,s)$, we eliminate the unknown coefficient $\mu(x)$ from equation (2.11) by differentiating (2.11), (2.12) with respect to the s-variable in accordance with [10] and [12]. As a result, we obtain the problem

$$q_{xx} + 2s^2 q_x v_x - 2sq_x = 2v_x - 2sv_x^2 \quad \text{in } (0,1), \ s \in [\underline{s}, \overline{s}], \tag{2.13}$$

$$q(0,s) = v_0'(s), \quad q_x(0,s) = v_1'(s), \tag{2.14}$$

$$q_x(1,s) = 0. \tag{2.15}$$

Note that the condition (2.15) follows directly from (2.8), because $\mu(x) = 1$ outside of the interval $(0,1)$ and

$$v(x,s) = -\int_s^{\overline{s}} q(x,\tau)\, d\tau + v(x,\overline{s}), \tag{2.16}$$

where

$$v(x,\overline{s}) = -\int_{\overline{s}}^{\infty} q(x,\tau)\, d\tau$$

3. Description of the algorithm. It follows from the previous section that if both functions $q(x,s)$ and $v(x,s)$ are known, then the solution of GCIP can be found in the closed form from the equation (2.11). However, these functions are unknown. If one knows an approximate solution $(\tilde{q}, \tilde{v})$ to this problem, then the approximate solution $\tilde{\mu}(x)$ of the generic inverse problem is given by

$$\tilde{\mu}(x) \approx \tilde{v}_{xx} + s^2 \tilde{v}_x^2 - 2s\tilde{v}_x + 1. \tag{3.1}$$

Thus, determining the approximate solution of the problem (2.13)-(2.15) plays the crucial role in developing the reconstruction algorithm.

Note that if the function $v(x,s)$ is given, then the problem (2.13)-(2.15) is linear with respect to $q(x,s)$. It may seem, therefore, that in order to produce an approximate solution to this problem, one may solve a traditional boundary value problem for the second-order ODE (2.13) with two boundary conditions (2.14) and (2.15). However, since $q(x,s)$ depends on $v(x,s)$, one needs to iterate both functions q and v. In this case, the sucessive approximations may not converge to the appropriate approximations of $q(x,s)$ and $v(x,s)$. This fact was observed in [10] as well as in our numerical experiments when attempting to solve the traditional BVP. Therefore, the method of quasi-reversibility (see, e.g., [14]), which is well suited to handle overdetermined boundary value problems, has been used for the approximate solution of the problem (2.13)-(2.15). Let the function $v(x,s)$ be fixed for any fixed parameter $s \in [\underline{s}, \overline{s})$, and the left- and right-hand sides of the equation (2.13) be denoted as

$L(q)(x)$ and $F(x)$. Then the method of quasi-reversibility consists of minimizing the Tikhonov functional

$$T_\lambda(q) = \|L(q)(x) - F(x)\|^2_{L_2(0,1)} + \lambda\|q\|^2_{H^2(0,1)}, \tag{3.2}$$

where $\lambda > 0$ is the regularization parameter, subject to the boundary conditions (2.14) - (2.15). It was shown in [12] that this functional has a unique minimizer. Furthermore, since this functional is the sum of squares of two expressions, which depend linearly on the function q , it is strictly convex. This means that any numerical method, such as the gradient or Newton-like one, allows for determining numerically that unique minimizer q_λ of the functional $T_\lambda(q)$ for every $s \in [\underline{s}, \overline{s}]$. However, it should be emphasized that in accordance with the theory of ill-posed problems (see, e.g., [29]), the regularization parameter λ must be chosen consistently with the level of noise δ in the "measured" data $\tilde{\varphi}(s)$, i.e., such that $\|\varphi - \tilde{\varphi}\|_{C[\underline{s},\overline{s}]} \leq \delta$, in order to ensure the regularizing property. A priori parameter choice $\lambda(\delta) = \delta^{2\nu}$, where $\nu \in (0,1)$ (see, e.g., [25, 29]) is recommended for use.

The regularization procedure described above allows us to solve numerically the problems (2.13) - (2.15) only if the function $v(x,s)$ is known. However, in reality both functions $q(x,s)$ and $v(x,s)$ are unknown. To overcome this difficulty, we determine the successive approximations of these functions as follows. We first utilize the asymptotic behavior of $v(x,s)$. It follows from [10] (see Lemma 2.1) that there exists a function $p(x) \in C^{2+\alpha}[0,1]$, such that

$$v(x,s) = \frac{p(x)}{s} + O\left(\frac{1}{s^2}\right), s \to \infty, x \in [0,1].$$

Since $q(x,s) = \partial_s v(x,s)$, we obtain for sufficiently large s

$$v(x,s) \approx \frac{p(x)}{s}, q(x,s) \approx -\frac{p(x)}{s^2}. \tag{3.3}$$

Because of asymptotics (3.3), we choose $s = \overline{s}$ and substitute these representations in (2.13) - (2.15). As a result, we obtain the following problem

$$p_{xx}(x) = 0 \ \text{ in } (0,1), \tag{3.4}$$

$$p(0) = -\overline{s}^2 v_0'(\overline{s}),\ p'(0) = -\overline{s}^2 v_1'(\overline{s}),\ p'(1) = 0. \tag{3.5}$$

This problem is also overdetermined.

Initialization. We solve numerically the problem (3.4)-(3.5) by the method of quasi-reversibility. Denote $p_{QRM}(x)$ its solution. Then we determine the initial approximation of the function $v(x,s)$ as

$$v^{(0)}(x,s) = \frac{p_{QRM}(x)}{s},\ x \in [0,1],\ s \in [\underline{s}, \overline{s}]. \tag{3.6}$$

Clearly, the initial approximations of the functions $u(x,s)$ and $q(x,s)$ will be $u_0(x,s)$ and $q^0(x,s) = -p_{QRM}(x)/s^2$.

Step 1. Beginning with $v^0(x,s)$, we start the iterative process. Assume that the kth successive approximation $v^{(k)}(x,s)$ has been determined for all parameters $s \in [\underline{s}, \overline{s})$. Then, given $v^{(k)}(x,s)$, we solve the overdetermined problem for $q^{(k+1)}$

$$\begin{aligned} &\partial_x^2 q^{(k+1)}(x,s) + 2s^2 \partial_x q^{(k+1)}(x,s)\partial_x v^{(k)}(x,s) - 2s\partial_x q^{(k+1)}(x,s) \\ &= 2\partial_x v^{(k)}(x,s) - 2s(\partial_x v^{(k)}(x,s))^2 \ \text{ in } (0,1), \\ &q^{(k+1)}(0,s) = \varphi_0'(s), \ \ \partial_x q^{(k+1)}(0,s) = \varphi_1'(s), \partial_x q^{(k+1)}(1,s) = 0 \end{aligned}$$

for each fixed parameter $s \in [\underline{s}, \overline{s})$ and find the successive approximation $q^{k+1}(x,s)$.
Step 2. We use the formula (2.16) to update the function $v(x,s)$ for each parameter $s \in [\underline{s}, \overline{s})$ as follows.

$$v^{(k+1)}(x,s) = -\int_s^{\overline{s}} q^{(k+1)}(x,\nu)d\nu + v^{(k)}(x,\overline{s}), \tag{3.7}$$

$$\partial_x v_x^{(k+1)}(x,s) = -\int_s^{\overline{s}} \partial_x q^{(k+1)}(x,\nu)d\nu + \partial_x v^{(k)}(x,\overline{s}), \tag{3.8}$$

$$\partial_x^2 v^{(k+1)}(x,s_{n-1}) = -\int_s^{\overline{s}} \partial_x^2 q^{(k+1)}(x,\nu)d\nu + \partial_x^2 v^{(k)}(x,\overline{s}). \tag{3.9}$$

Step 3. Let $s^* \in [\underline{s}, \overline{s})$ be a certain number which is independent on k. We update the coefficient as

$$\mu_{k+1}(x) = \partial_x^2 v^{(k+1)}(x,s^*) + (s^*)^2(\partial_x v^{(k+1)}(x,s^*))^2 - 2s^*\partial_x v^{(k+1)}(x,s^*) + 1, \tag{3.10}$$

where $x \in (0,1)$, and set $\mu_{k+1}(x) = 1$ for $x = 0$ and $x = 1$.
Step 4. Update the function $v(x,\overline{s})$ and its derivatives by solving the forward problem

$$\partial_x^2 u^{(k+1)}(x,\overline{s}) - \overline{s}^2\mu_{k+1}(x)u(x,\overline{s}) = -\delta(x-x_0), \quad x \in (0,1),\ x_0 \notin (0,1), \tag{3.11}$$

$$\lim_{|x|\to\infty} u^{(k+1)}(x,\overline{s}) = 0 \tag{3.12}$$

and determining the functions

$$v^{(k+1)}(x,\overline{s}) = \frac{\ln u^{(k+1)}(x,\overline{s})}{\overline{s}^2} - \frac{x-x_0}{\overline{s}} - \frac{\ln 2\overline{s}}{\overline{s}^2}, \tag{3.13}$$

$$\partial_x v^{(k+1)}(x,\overline{s}) = \frac{\partial_x u^{(k+1)}(x,\overline{s})}{\overline{s}^2 u^{(k+1)}(x,\overline{s})} - \frac{1}{\overline{s}}, \tag{3.14}$$

$$\partial_x^2 v^{(k+1)}(x,\overline{s}) = \frac{\partial_x^2 u^{(k+1)}(x,\overline{s})}{\overline{s}^2 u^{(k+1)}(x,\overline{s})} - \left(\frac{\partial_x u^{(k+1)}(x,\overline{s})}{\overline{s}u^{(k+1)}(x,\overline{s})}\right)^2 \tag{3.15}$$

for $x \in [0,1]$. It follows from (3.7)-(3.9) that knowledge of the function $v^{(k+1)}(x,\overline{s})$ and its derivatives is crucial in reconstructing $\mu(x)$ via the formula (3.10).
Stopping criterion. The iterative process continues until a stopping criterion is fulfilled. If the level of noise δ in the data $\varphi(s)$ is given or it can be estimated, then it is natural to stop the process at the iterate

$$k_{stop} = \min\left\{k : \|\partial_x u_{\mu_k}(0,s) - \tilde{\varphi}(s)\|_{L_2[\underline{s},\overline{s}]} \le \delta\right\}, \tag{3.16}$$

where the function $u_{\mu_k}(x,s)$ is determined by solving the forward problem (2.7)-(2.8) with $\mu(x) = \mu_k(x)$ for every successive approximation $\mu_k(x)$. Note that since the norm in (3.16) represents the residual functional on $\mu_k(x)$, the number k_{stop} plays the role of the regularization parameter. In this case, the closeness of $\mu_{k_{stop}}(x)$ to the true coefficient $\mu(x)$ needs to be estimated. Also, we note that in computing we deal with the discrete functions defined on grids with respect to both variables x and s. In this case, the derivatives are approximated by their finite difference analogous and the integrals in (3.7)-(3.9) - by appropriate quadratures.

4. Convergence of successive approximations. Let $\underline{s} > 0, \overline{s} > 1$. Let $\mu^*(x)$ be the unique solution of the GCIP satisfying conditions (2.6) and corresponding to the data $\varphi(s)$, $s \in [\underline{s}, \overline{s}]$. In the convergence analysis we assume that all successive approximations $\mu_k(x)$ obtained by the algorithm described in the section 3 also satisfy the conditions (2.6). In addition, following (2.10) and (3.3), we assume that the function $v(x,s) = s^{-2} \ln(u/u_0)$ can be represented as

$$v(x,s) = \frac{p(x)}{s}, \forall s \geq \overline{s}, \tag{4.1}$$

where the function $p \in C^{2+\alpha}[0,1]$. Let $h > 0$ be the largest distance between two adjacent nodes in a grid with respect to the s-variable. Let $\chi \in (0,1)$ be a given real number, such that $\|\varphi - \tilde{\varphi}\|_{C[\underline{s},\overline{s}]} \leq \chi$, where $\tilde{\varphi}(s)$ is the single boundary measurement. Denote $\eta = \max(\delta, h)$. Then the following analogue of Theorem 6.1 in [12] takes place.

THEOREM 4.1. *If the initial approximation $v^{(0)}(x,s)$ in the proposed algorithm is determined as in (3.6), and the regularization parameter λ in the Tikhonov's functional (3.2) is chosen as $\lambda = \chi^2$, then there exists a constant $C = C(x_0, m, \overline{s})$, such that for η chosen from*

$$\eta < \frac{1}{C^{k_{stop}}}$$

the following inequality is fulfilled for all $k \in [1, k_{stop}]$

$$\|\mu_k(x) - \mu^*(x)\|_{L_2(0,1)} \leq \eta^\gamma, \ \gamma \in (0,1), \tag{4.2}$$

where the number γ does not depend on $k, h, \chi, \mu_k(x)$ and $\mu^*(x)$.

Proof. Since the arguments are analogous to those used for the proof of Theorem 6.1 of [12], we only outline the scheme of the proof. First, using (3.4)-(3.6), (4.1) and Lemma 6.1 in [12], it is shown that

$$\max_{s \in [\underline{s}, \overline{s}]} \left\| v^{(0)}(x,s) - v(x,s) \right\|_{H^2(0,1)} \leq C\eta. \tag{4.3}$$

Recall that m is the constant in (2.6). Consider the solution $u_{\overline{\mu}}(x,s)$ of the problem (2.7), (2.8) for the case $\mu(x) \equiv m$,

$$u_m(x,s) = \frac{\exp(-s\sqrt{m}\,|x - x_0|)}{2s}.$$

Then it follows from [12]

$$u_m(x,s) < u(x,s) \leq u_0(x,s), \forall x \in [0,1], \forall s \in [\underline{s}, \overline{s}]. \tag{4.4}$$

Using (4.4), as well as estimates of a minimizer of the functional (3.2) indicated in Lemma 5.2 in [12], one can estimate norms $\left\| q_n^{(1)} - q_n \right\|_{H^2(0,1)}, n \in [1, N]$. Next, using (3.7) - (3.15) and (4.3), one can obtain the estimate (4.2) for $k = 1$. Next, using the latter estimate as well as (4.4), one can obtain an analogue of (4.3) for $\max_{s \in [\underline{s}, \overline{s}]} \left\| v^{(1)}(x,s) - v(x,s) \right\|_{H^2(0,1)}$. Finally, we can continue this process in a similar way until it stops at $k = k_{stop}$. □

The main consequence of this theorem that it guarantees a good approximation of the true solution μ^* regardless *a priori* knowledge of a small neigborhood of this solution.

5. Refinement of $\mu_{k_{stop}}$. The theorem 4.1 guarantees an appropriate closeness of successive approximations to the true coefficient only if numbers χ and h are sufficiently small. In practice, however, it is more typical than exceptional that the level of noise χ in the experimental data is fixed and it is not small enough. In this case, the approximation $\mu_{k_{stop}}(x)$ may not possess high spatial and contrast resolutions, i.e., the quantitative imaging may be problematic. To alleviate this restriction, we propose to take advantage of knowledge of not only $\mu_{k_{stop}}(x)$ but also the field $v^{(k_{stop})}(x,s)$ everywhere in $[0,1]$. Indeed, we observe that given $v^{(k_{stop})}(x,s)$, one can determine from (2.10) the function

$$u^{(k_{stop})}(x,s) = u_0(x,s)\exp\left[s^2 v^{(k_{stop})}(x,s)\right]. \tag{5.1}$$

Choose a parameter $s_* \in [\underline{s},\overline{s})$ and denote $\tilde{u}(x,s_*) = u^{(k_{stop})}(x,s_*)$ the interior data. We observe that although the function $\tilde{u}(x,s_*)$ may be close to the solution of (2.7)-(2.8), it does not satisfy this problem. This observation makes it possible matching the interior field $\tilde{u}(x,s_*)$ with the function $u_\mu(x,s_*)$ with the hope of improving the approximation $\mu_{k_{stop}}(x)$. Here, $u_\mu(x,s), s \in [\underline{s},\overline{s}]$ is the solution of the problem (2.7)-(2.8) that corresponds to the function $\mu(x)$ satisfying conditions (2.6).

Although the results established below remain valid in the Banach spaces, we consider the finite-dimensional Hilbert spaces in view of their use in scientific computing. Let H be such a space. As an example, we indicate the subspace of the space $L_2(R)$ spanned by a finite number of piecewise linear finite elements vanished outside of the interval $(0,1)$. For every function $\mu(x)$ satisfying conditions (2.6) denote $\mu(x) - 1 = \overline{\mu}(x) \in L_2(R)$. Let $G \subset H$ be the set of such functions. Clearly, G is bounded in the space H. Consider the map $F : \overline{G} \to L_2(0,1)$, where

$$F(\overline{\mu}) = u_\mu(x,s_*), x \in (0,1), \forall \overline{\mu}(x) = \mu(x) - 1 \in G.$$

It follows from (2.7) that the operator F is one to one. Denote $K = F\left(\overline{G}\right)$ the range of F. Since $\overline{G}$ is a compact set in H, then the Tikhonov's theorem [3], [29] implies that the inverse operator $F^{-1} : K \to \overline{G}$ is continuous. Let $\omega_F(z), z \in \{z \geq 0\}$ be the modulo of continuity of the operator F^{-1} on the set K. Then

$$\|\overline{\mu}_1 - \overline{\mu}_2\|_H \leq \omega_F\left(\|F(\overline{\mu}_1) - F(\overline{\mu}_2)\|_{L_2(0,1)}\right), \forall \overline{\mu}_1, \overline{\mu}_2 \in \overline{G}. \tag{5.2}$$

In the GCIP both functions $\mu^*(x)$ and $u^*_{\mu^*}(x,s_*)$ are supposed to be unknown. Instead, their approximations $\tilde{\mu} = \mu_{k_{stop}}(x) \in G$ (see (4.2)) and $\tilde{u}(x,s_*) \in L_2(0,1)$ are given, such that

$$\|u^*_{\mu^*}(x,s_*) - \tilde{u}(x,s_*)\|_{L_2(0,1)} \leq \varrho, \tag{5.3}$$

where $\varrho = C\eta^{gamma}$, $C = const > 0$. We are interested in finding a new approximation of $\mu^*(x)$ that would be more close to it than the approximation $\mu_{k_{stop}}(x)$.

Consider the Tikhonov functional

$$T_\lambda(\overline{\mu}) = \|F(\overline{\mu}) - \tilde{u}(x,s_*)\|^2_{L_2(0,1)} + \lambda\|\overline{\mu} - \overline{\mu}_{k_{stop}}\|^2_H, \tag{5.4}$$

where $\overline{\mu}, \overline{\mu}_{k_{stop}} \in \overline{G}$. Since $\overline{G}$ is a bounded compact set in the finite dimensional space H, then it follows from the Weierstrass theorem that for any $\lambda > 0$ there exists a minimizer $\mu_\lambda(x) \in \overline{G}$ of the functional (5.4), i.e.,

$$\mu_\lambda(x) = argmin\left\{T_\lambda(\mu) : \overline{\mu} \in \overline{G}\right\}.$$

Moreover, one can show that the map F has the Lipshitz-continuous Fréchet derivative. Then, it follows from Theorem 1.9.1.2 in [3] that the Tikhonov's functional $T_\lambda(\overline{\mu})$ is strictly convex in a sufficiently small neighborhood of the function $\overline{\mu}^*$. This property allows for establishing convergence of $\mu_\lambda(x)$ to $\mu^*(x)$. For any positive real number a and any $x \in H$ we denote $\mathcal{U}_a(x) = \{z \in H : \|x - z\| < a\}$ the a - neighborhood of the element x. Then the following theorem takes place.

THEOREM 5.1. *Let $\lambda = \lambda(\varrho) = \varrho^{2\nu}, \nu \in (0, 1/2)$, and $\xi \in (0,1)$ be an arbitrary number. Then there exists a sufficiently small number $\varrho_0 = \varrho_0(H, m, \nu, \xi)$ such that for all $\varrho \in (0, \varrho_0)$*

$$\left\|\overline{\mu}_{\lambda(\delta)} - \overline{\mu}^*\right\|_H \leq \begin{cases} \xi\|\overline{\mu}^* - \overline{\mu}_{k_{stop}}\|_H, & \text{if } \overline{\mu}_{k_{stop}} \neq \overline{\mu}^*, \\ \xi, & \text{if } \overline{\mu}_{k_{stop}} = \overline{\mu}^*. \end{cases} . \tag{5.5}$$

If $\nu \in (0, 1/4)$, then there exists a sufficiently small number $\overline{\varrho} = \overline{\varrho}(H, m, \nu) \in (0,1)$ such that for every $\varrho \in \left(0, \overline{\delta}\right)$ the functional (5.4) is strictly convex in the neighborhood $\mathcal{U}_{\varrho^{3\nu}}(\overline{\mu}^*)$. If the solution $\mu_{k_{stop}}$ is so accurate that $\|\overline{\mu}^* - \overline{\mu}_{k_{stop}}\|_H < \varrho^{3\nu}/3$, then $\overline{\mu}_{\lambda(\varrho)} \in \mathcal{U}_{\varrho^{3\nu}/3}(\overline{\mu}^*)$, and any gradient or Newton-like method of minimization of $T_\lambda(\overline{\mu})$ with the initial approximation $\mu_{k_{stop}}$ converges to $\overline{\mu}_{\lambda(\varrho)}$.

Proof. Since the arguments established in [8] and in theorems 1.8 and 1.9.1.2 of [3] work for this proof, we only prove (5.5). We have

$$\left\|F\left(\overline{\mu}_{\lambda(\delta)}\right) - F\left(\overline{\mu}^*\right)\right\|_{L_2(0,1)} \leq \left\|F\left(\overline{\mu}_{\lambda(\delta)}\right) - \tilde{u}\left(x, s_*\right)\right\|_{L_2(0,1)} + \|F\left(\overline{\mu}^*\right) - \tilde{u}\left(x, s_*\right)\|_{L_2(0,1)}.$$

Hence, (5.3) implies that

$$\left\|F\left(\overline{\mu}_{\lambda(\delta)}\right) - F\left(\overline{\mu}^*\right)\right\|_{L_2(0,1)} \leq \left\|F\left(\overline{\mu}_{\lambda(\delta)}\right) - \tilde{u}\left(x, s_*\right)\right\|_{L_2(0,1)} + \varrho. \tag{5.6}$$

We now estimate the first term in the right hand side of (5.6). Since ϱ is sufficiently small, $\varrho^2 < \varrho^{2\nu}$. Hence, we have

$$\begin{aligned} \left\|F\left(\overline{\mu}_{\lambda(\varrho)}\right) - \tilde{u}\left(x, s_*\right)\right\|^2_{L_2(0,1)} &\leq T_{\lambda(\varrho)}(\overline{\mu}_{\lambda(\varrho)}) \leq T_{\lambda(\delta)}(\overline{\mu}^*) \\ &\leq \varrho^2 + \varrho^{2\nu}\|\overline{\mu}^* - \overline{\mu}_{k_{stop}}\|^2_H \leq \varrho^{2\nu}\left(1 + \|\overline{\mu}^* - \overline{\mu}_{k_{stop}}\|^2_H\right). \end{aligned}$$

Then we obtain

$$\left\|F\left(\overline{\mu}_{\lambda(\varrho)}\right) - F\left(\overline{\mu}^*\right)\right\|_{L_2(0,1)} \leq \varrho^\nu\sqrt{1 + \|\overline{\mu}^* - \overline{\mu}_{k_{stop}}\|^2_H} + \varrho \leq 2\varrho^\nu\sqrt{1 + \|\overline{\mu}^* - \overline{\mu}_{k_{stop}}\|^2_H}.$$

Using (5.2), we obtain

$$\left\|\overline{\mu}_{\lambda(\varrho)} - \overline{\mu}^*\right\|_H \leq \omega_F\left(2\varrho^\nu\sqrt{1 + \|\overline{\mu}^* - \overline{\mu}_{k_{stop}}\|^2_H}\right). \tag{5.7}$$

We first consider the option $\overline{\mu}_{k_{stop}} \neq \overline{\mu}^*$. Since $\lim_{z \to 0^+}\omega_F(z) = 0$, then we can find such number $\varrho_0 = \varrho_0(H, m, \nu, \xi) \in (0,1)$ that for all $\varrho \in (0, \varrho_0)$

$$\omega_F\left(2\varrho^\nu\sqrt{1 + \|\overline{\mu}^* - \overline{\mu}_{k_{stop}}\|^2_H}\right) \leq \xi\|\overline{\mu}^* - \overline{\mu}_{k_{stop}}\|_H. \tag{5.8}$$

Combining (5.7) and (5.8), we obtain the inequality (5.5). The second option can be considered by analogy. ∎

Note that although the theorem 5.1 does not allow for the quantitative estimate of the distance between μ^* and μ_λ, it justifies the use of the Tikhonov regularization with the interior data for refining $\mu_{k_{stop}}$.

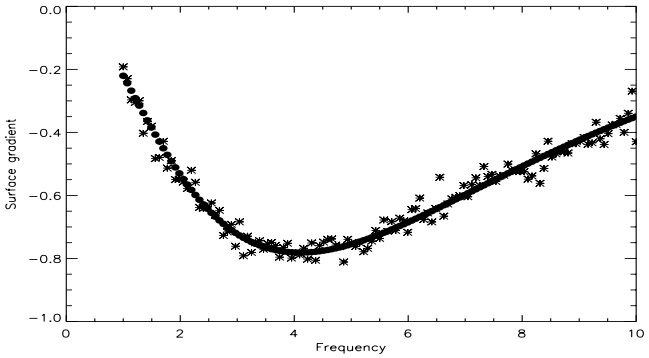

FIG. 5.1. *The simulated electromagnetic frequency data* $\overline{\varphi}(s)$ *in the interval* $[1, 10]$. *The noiseless data is shown by bullets and the data corrupted by noise at the level of* 5% *is shown by asterisks.*

6. Numerical study. In this section we perform some numerical experiments in order to demonstrate the computational effectiveness of the proposed algorithm. For this purpose, we show how it can be applied to frequency sounding and electrical prospecting of layered media.

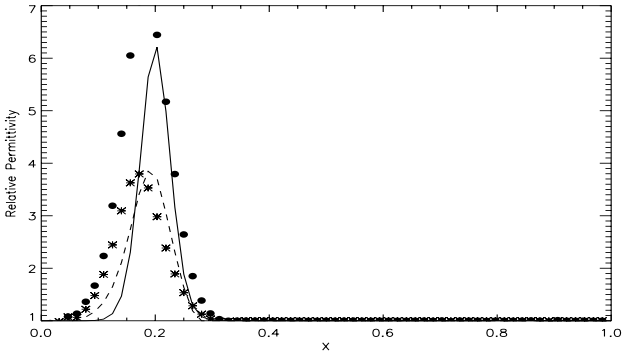

FIG. 6.1. *Reconstructions of the relative electrical permittivity of a single mid-contrast land mine in the air: (1) without refinement (dashed), (2) with refinement using the boundary data (asterisks), (3) with refinement using the interior data (bullets). The original distribution is shown by a solid line.*

6.1. Frequency sounding. Without loss of generality, we consider frequency sounding of layered media and exploit its mathematical model developed in [24]. In accordance with this model, a pulsed plane wave, which is normally incident at the plane $z = 0$, propagates through an inhomogeneous layer whose material property depends continuously on one variable z only and it is supposed to be constant outside of the interval $(0, L)$. The propagation and scattering of such a pulsed plane wave can be described by the following initial boundary value problem

$$c^{-2}(z)U_{tt} - U_{zz} = 0, \quad z > 0, \quad t > 0, \tag{6.1}$$

$$U(z, 0) = U_t(z, 0) = 0, \tag{6.2}$$

$$U(0, t) = \delta(t). \tag{6.3}$$

If the incident wave is electromagnetic and a medium is dielectric, the scalar quantity $U(z,t)$ can be interpreted as an appropriate component of the electric field propagating with the speed $c(z) = 1/\sqrt{\mu_0 \mu \varepsilon_0 \varepsilon(z)}$. Here, $\varepsilon(z)$ and μ are relative permittivity and permeability of the inhomogeneous layer and ε_0 and μ_0 are absolute permittivity and permeability of vacuum. If the incident wave is acoustic, the quantity $U(z,t)$ can be interpited as the acoustic potential and $c(z)$ is the sound speed.

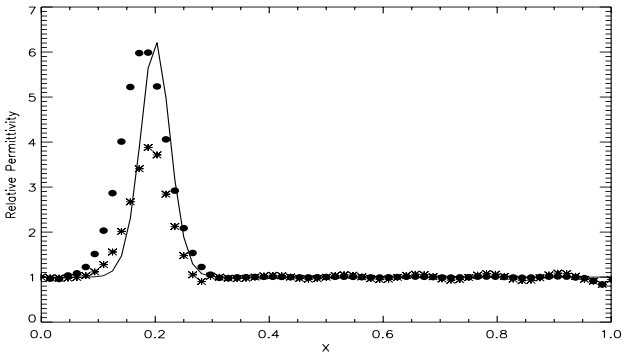

FIG. 6.2. *Recovering the relative electrical permittivity of a single mid-contrast land mine from the perturbed data (the level of noise is 5%) without refinement (asterisks) and with refinement (bullets).*

Inverse Problem of Frequency Sounding. *Let the function $U(z,t)$ be the solution of the initial boundary value problem (6.1)-(6.3). Given the function $U_z(0,t) = \Psi(t), t > 0$ and parameters $c_0 > 0, L > 0$, such that $c(z) = c_0$ for $z \geq L$, find the variable speed $c(z)$ on $(0,L)$.*

The traditional approach to this inverse problem consists of reducing the wave equation (6.1) to the Helmholtz equation by performing the Fourier transform and solving it by some globally convergent algorithms. To the author's knowledge, there are three groups of such algorithms. The algorithms of the first group are based on the so-called trace (asymptotic) formulae (see, e.g., [5]). The algorithms of the second group utilize the nonlinear Riesz transform allowing for reducing to an equivalent Volterra integral equation [23]. The algorithms of the third group are based on the convexification method [7]. Unlike the traditional approach, in [2], [3], [10], [11], [12], and [24] the Laplace transform was applied to an initial-boundary value problem for the wave equation. It was resulted in several other globally convergent algorithms.

Following the latter approach, we apply the Laplace transform

$$\overline{u}(z,\nu) = \int_0^\infty e^{-\nu t} U(z,t) dt, \quad z > 0, \quad \nu > \nu_0$$

to the problem (6.1)-(6.3) and introduce the dimensionless variables $x = z/L, s = \nu L/c_0, n(x) = c_0/c(Lx)$. Denoting $u(x,s) = \overline{u}(Lx, c_0 s/L)$, we obtain the dimensionless two-point problem for the second-order ordinary differential equation

$$u_{xx}(x,s) - s^2 n^2(x) u(x,s) = 0, \quad x \in (0,1), \quad s \in [\underline{s}, \overline{s}], \tag{6.4}$$

$$u(0,s) = 1, \tag{6.5}$$

$$u_x(1,s) + s u(1,s) = 0. \tag{6.6}$$

It should be emphasized that if we consider the equation (6.1) for any $z \in (-\infty, \infty)$ together with the condition $U_t(z,0) = \delta(z - z_0), z_0 < 0$, then we obtain the GCIP formulated in the section 2. In this case, the transmission condition (6.6) follows from the radiation condition $\lim_{x\to\infty} u(x,s) = 0$ and $n(x) \equiv 1$ for $x > 1$. It follows from [24] that for a sufficiently smooth refraction coefficient $n(x)$ the problem (6.4)-(6.6) has a unique solution. Therefore, the inverse problem of frequency sounding can be reformulated as follows.

Let the function $u(x,s)$ be the solution of the problem (6.4)-(6.6) that corresponds to $n(x)$, but $u_x(0,s)$ is unknown. Instead, an approximation $\overline{\varphi}(s), s \in [\underline{s}, \overline{s}], \underline{s} > 0$ of $u_x(0,s)$ and the real number $\delta > 0$ are given, such that $\|u_x(0,s) - \varphi(s)\|_{L_2[\underline{s},\overline{s}]} \leq \delta$. Find an approximation of $n(x)$ in $(0,1)$.

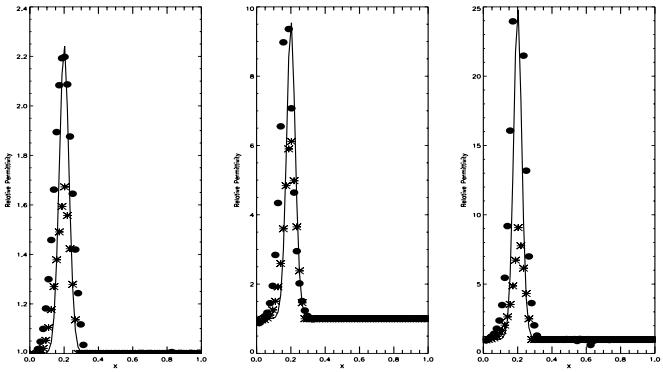

FIG. 6.3. *Reconstructions of the relative electrical permittivity of a single low-contrast (left), mid-conrast (middle) and high-contrast (right) land mine in the air. The results of reconstruction are shown by asterisks (without refinement) or by bullets (with refinement). The original distribution is shown by a solid line.*

To generate the frequency sounding data $\overline{\varphi}(s)$, we first simulated numerically the data for a given $n(x)$. To provide a high accuracy of reconstruction, we represented the solution of the problem (6.4)-(6.6) in the form $u = u_e + \overline{u}$, where $u_e = e^{-sx}$ is its solution for $n(x) \equiv 1$. Thus we solved numerically the boundary value problem

$$\overline{u}_{xx}(x,s) - s^2 n^2(x)\overline{u}(x,s) = -s^2 e^{-sx}(1 - n^2(x)), \quad x \in (0,1), \quad s \in [\underline{s}, \overline{s}], \tag{6.7}$$

$$\overline{u}(0,s) = 0, \tag{6.8}$$

$$\overline{u}_x(1,s) + s\overline{u}(1,s) = 0. \tag{6.9}$$

The second-order finite-difference analogue of this problem was numerically solved by a stable version of the elimination method (see [19]). Note that since the solution of this difference problem approximates the solution of the problem (6.7)-(6.9), the function $\overline{\varphi}(s)$ approximates $\overline{u}_x(0,s)$. The level of error of this approximation depends on several factors, such as smoothness of the refraction coefficient, grid, CPU, etc. In the numerical experiments, we utilized the uniform grids containing from 64 to 100 nodes, and the refraction coefficient was assumed to be either smooth or piecewise-constant. Under such conditions, it was estimated from comparison with the model refraction coefficients that the level δ varied approximately from $5 \cdot 10^{-6}$ (if $n(x)$ is smooth) to $5 \cdot 10^{-4}$ (if $n(x)$ is piecewise-constant).

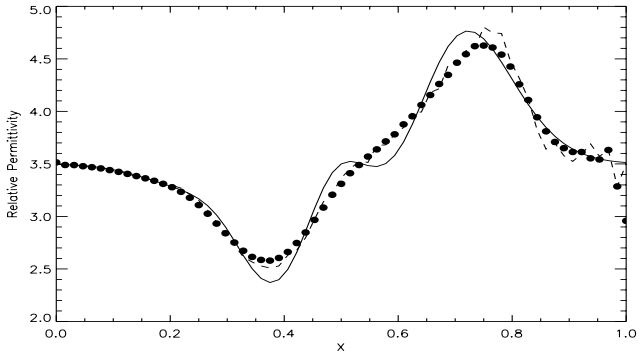

FIG. 6.4. *Reconstructions of the relative electrical permittivity of the model clutter without (asterisks) and with (bullets) refinement. The original distribution is shown by a solid line.*

Since $v = \overline{v} - x/s$ and $q = \overline{q} + x/s^2$, where

$$\overline{v} = \frac{\ln\left(\overline{u} + e^{-sx}\right)}{s^2} + \frac{x}{s} \text{ and } \overline{q} = \partial_s \overline{v},$$

the two-point problem for the function $\overline{q}$ has the form

$$\overline{q}_{xx}(x,s) + 2s(s\overline{v}_x - 1)\overline{q}_x(x,s) = F(\overline{v}_x; x, s), \quad x \in (0,1), \quad s \in [\underline{s}, \overline{s}], \tag{6.10}$$

$$\overline{q}(0,s) = 0, \tag{6.11}$$

$$\overline{q}_x(1,s) = 0, \tag{6.12}$$

where $F(\overline{v}_x; x, s) = -2\overline{v}_x(s\overline{v}_x - 1)$. The boundary data is given by

$$\overline{q}_x(x,0) = \overline{\psi}(s) = \partial_s \left(\frac{\overline{\varphi}(s)}{s^2}\right). \tag{6.13}$$

In computing, the operator ∂_s is understood in the sense of differentiating an interpolating cubic spline of $\overline{\varphi}(s)$. We emphasize that the nonlinear problem (6.10)-(6.13) has two unknowns $(\overline{v}, \overline{q})$, and it looks similar to the problem (2.13) - (2.15). Therefore, we applied the algorithm described in the section 3. Indeed, to start the iterative process, we let $\overline{v}^{(0)}(x,s) = \overline{p}_{QRM}(x)$, where $\overline{p}_{QRM}(x)$ is the solution of the problem

$$p_{xx} = 0, \quad x \in (0,1), \tag{6.14}$$

$$p(0) = p_x(1) = 0, \tag{6.15}$$

$$p_x(0) = -\overline{s}^2 \overline{\psi}(\overline{s}) \tag{6.16}$$

obtained by the method of quasi-reversibility. Suppose that after k iterates the approximation $\overline{v}^{(k)}(x,s)$ is obtained. Then solving the problem (6.10)-(6.12) with the boundary data $\overline{\psi}(s)$ by the quasi-reversibility method as described in the section 3, we obtained the corresponding approximation $\overline{q}^{(k)}(x,s)$. Given both these approximations, we updated the refraction coefficient as follows.

$$n^2_{k+1}(x) = 1 + \left(G_k(x) - 2s^* H_k(x) + s^* H^2_k(x)\right),$$

where

$$H_k(x) = -\int_{s^*}^{\overline{s}} \overline{q}^{(k)}_x(x,\nu)d\nu + \overline{v}^{(k)}_x(x,\overline{s}),$$

$$G_k(x) = -\int_{s^*}^{\overline{s}} \overline{q}_{xx}^{(k)}(x,\nu)d\nu + \overline{v}_{xx}^{(k)}(x,\overline{s}).$$

In the numerical experiments the integrals were approximated by a quadrature formula. It should also be mentioned that although from a theoretical standpoint, the parameter s^* can be chosen arbitrarily, in the numerical experiments it was chosen to provide the best accuracy of reconstruction of some benchmark refraction coefficients. The function $\overline{v}(x,\overline{s})$ at $\overline{s}$ was updated as follows. We first solve numerically the two-

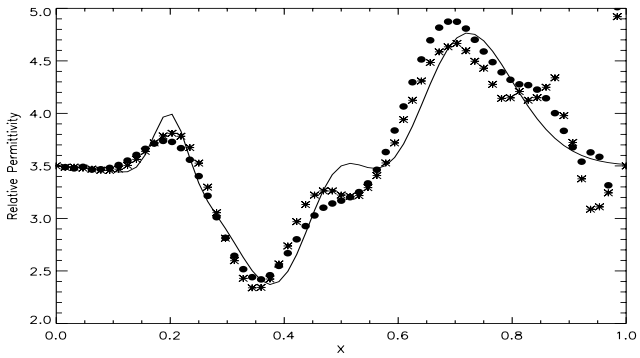

FIG. 6.5. *Reconstructions of the relative electrical permittivity of a low-contrast land mine embedded in clutter at $x = 0.2$ without (asterisks) and with (bullets) refinement. The original distribution is shown by a solid line.*

point problem (6.7) - (6.9) with the $(k+1)$th successive approximation $n_{k+1}(x)$ of the refraction coefficient. Let $\overline{u}^{(k+1)}(x,\overline{s})$ be such a solution. Then the updated function $\overline{v}(x,\overline{s})$ and its two derivatives were computed as

$$\overline{v}^{(k+1)}(x,\overline{s}) = \frac{\ln\left(\overline{u}^{(k+1)}(x,\overline{s}) + \exp\left(-\overline{s}x\right)\right)}{\overline{s}^2} + \frac{x}{\overline{s}},$$

$$\overline{v}_x^{(k+1)}(x,\overline{s}) = \frac{\overline{u}_x^{(k+1)}(x,\overline{s}) - \overline{s}e^{-sx}}{\overline{s}^2\left(\overline{u}^{(k+1)}(x,\overline{s}) + \exp\left(-\overline{s}x\right)\right)} + \frac{1}{\overline{s}},$$

$$\overline{v}_{xx}^{(k+1)}(x,\overline{s}) = \frac{\overline{u}_{xx}^{(k+1)}(x,\overline{s}) + \overline{s}^2e^{-sx}}{\overline{s}^2\left(\overline{u}^{(k+1)}(x,\overline{s}) + \exp\left(-\overline{s}x\right)\right)} - \left(\frac{\overline{u}_x^{(k+1)}(x,\overline{s}) - \overline{s}e^{-sx}}{\overline{s}\left(\overline{u}^{(k+1)}(x,\overline{s}) + \exp\left(-\overline{s}x\right)\right)}\right)^2.$$

Once the inequality

$$\|\partial_x \overline{u}_{n_k}(0,s) - \overline{\varphi}(s)\|_{L_2(\underline{s},\overline{s})} \leq \delta$$

was fulfilled, the iterative process was terminated. The approximate solution $n_{k_{stop}}(x)$ was refined as follows. We defined the function

$$\overline{u}^{(k_{stop})}(x,s_*) = u_0(x,s_*)\exp\left[s_*^2\overline{v}^{(k_{stop})}(x,s_*)\right] \tag{6.17}$$

and minimized the functional

$$J_\lambda(n) = \|\overline{u}_n(x,s_*) - \overline{u}^{(k_{stop})}(x,s_*)\|^2_{L_2(0,1)} + \lambda\|n(x) - n_{k_{stop}}(x)\|^2_{L_2(0,1)}. \tag{6.18}$$

Since the functional $J_\lambda(n)$ is strictly convex, the Powell method with the initial approximation $\overline{n}_\lambda(x)$ was used to find its minimizer.

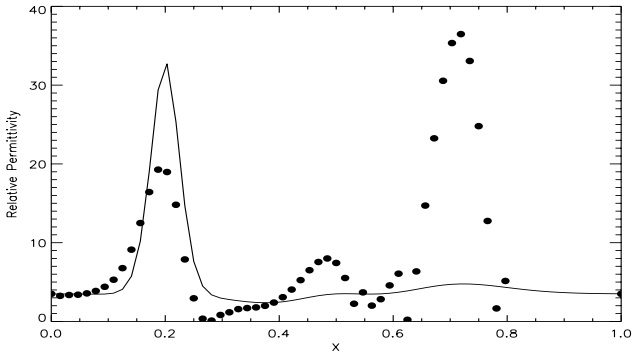

FIG. 6.6. *Reconstructions of the relative electrical permittivity of the model clutter without refinement (bullets). The original distribution is shown by a solid line.*

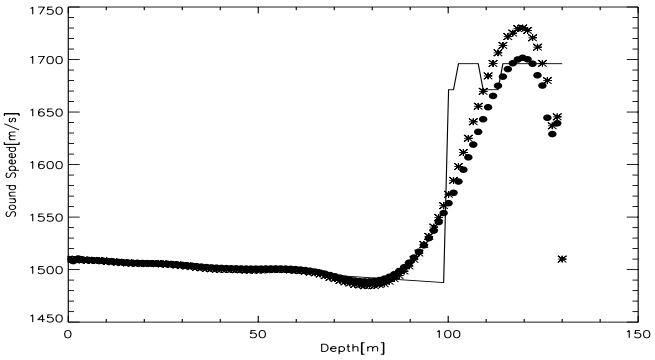

FIG. 6.7. *Results of recovering the sound speed profile from the data obtained on the see surface: reconstructions without (asterisks) and with (bullets) refinement. The original sound speed profile is shown by the solid line.*

6.1.1. Numerical results: electromagnetic frequency sounding. We simulated electromagnetic frequency sounding of dry layered soil, which is usually performed by ground penetrating radars for the purpose of land mine detection and classification. We assumed that the relative magnetic permeability and electrical permittivity of the background media are equal to 1, and $n(x) = \sqrt{\varepsilon(x)/\varepsilon_0}$. The realistic values of $n(x)$ (see, e.g., [32]) were used in the numerical experiments. The distribution of the relative electrical permittivity of a subsurface land mine was simulated by a Gaussian curve. Figure 5.1 shows the typical boundary data $\overline{\varphi}(s)$ generated by this mine embedded in the homogeneous background (air) with $\varepsilon = 1$. In Figure 6.1 it is shown the effect of refinement of $\varepsilon_\lambda(x)$ via fitting the interior data in comparison with refinement via fitting the boundary data. In this experiment, the non-perturbed frequency sounding data was used, and the regularization parameter λ providing the best accuracy was chosen $3.6 \cdot 10^{-3}$.

To demonstrate the robustness of the proposed algorithm, we simulated the perturbed data by adding the normally distributed noise to $\overline{\varphi}(s)$

$$\tilde{\varphi}(s) = \overline{\varphi}(s) + \gamma R,$$

where R is the normally distributed pseudo-random vector with mean zero and standard deviation of 1, and γ is the model standard deviation chosen as

$$\gamma = \epsilon \frac{\|\overline{\varphi}\|}{\|R\|},$$

where $\epsilon = \|\tilde{\varphi} - \overline{\varphi}\|/\|\overline{\varphi}\|$. The perturbed data is shown in Figure 5.1. Figure 6.2 shows the mean relative electrical permittivity obtained from samples containing twenty five realization of the pseudo-random vector R. Since robustness of the proposed algorithm was also confirmed in all other numerical experiemnts, we limit our next demonstrations by the results of recovering the material properties from the noiseless data. Since the land mines may be filled with the different explosives and they may

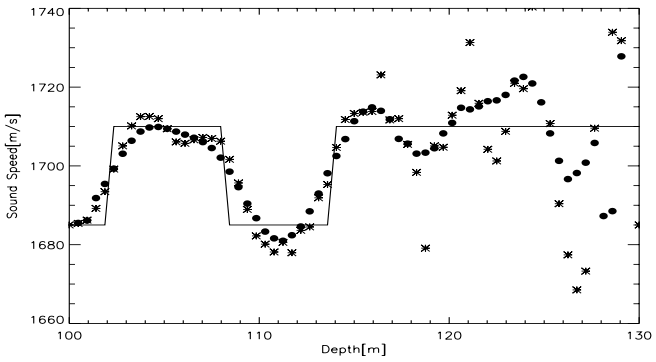

FIG. 6.8. *Results of recovering the sound speed profile from the data obtained on the see floor: reconstructions without (asterisks) and with (bullets) refinement. The original sound speed profile is shown by the solid line.*

be covered by either metallic or plastic materials, their averaged relative electrical permittivity may range from 2 to 25 or more units. Figure 6.3 shows the results of reconstruction for the different contrasts. In all such cases, the effect of refinement was significant.

In practice, even a near subsurface, where land mines are usually embedded in, is not homogeneous. This may be due to variations of sand and clay porosity, water saturation, presence of abris, etc. These inhomogeneities lead to unwanted variations in GPR signals that are referred to the clutter. We simulated the model clutter containing a continuously inhomogeneous layer with the relative electrical permittivity ranging from 2.4 to 4.75. Such a variation is typical, for instance, for a mixture of sand and clay with the variable porosity and water saturation. The results of reconstructions of the model clutter are shown in Figure 6.4. Also, we investigated how the presence of clutter affects reconstruction of the relative electrical permittivity of land mines. The results of reconstructions are shown in Figures 6.5 and 6.6. Clearly, the presence of clutter affects significantly the quality of quantitative imaging. Specifically, the higher the contrast the lower the quality, though a near surface land mine may still be detected and classified. Furthermore, we observed that refinement by fitting the interior data did not lead to a significant improvement if a low contrast land mine is embedded in clutter. In case of a high contrast land mine in clutter, refinement was not even possible.

6.1.2. Results of numerical experiments: acoustic frequency sounding. Also, we simulated acoustic frequency sounding of layered marine environments. In these cases, $n(z) = c_0/c(z)$, where $c(z)$ is the sound speed profile, and c_0 is the reference sound speed. In the numerical experiments, we used the values of parameters typical for the shallow waters and water-saturated sediments (see, e.g., [18]). To simulate the sound speed profile in the water column, we used the simplified Wilson's formula [31]

$$c(z) = 1449 + 4.6T(z) - 0.055T(z)^2 + 0.0003T(z)^3 = (1.39 - 0.12T(z))(S(z) - 35) + 0.017z,$$

where $T(z) = 20 - \beta z$ is the temperature (Celcius), z is the depth (m), and $S(z) = 34 + \tau z$ is the salinity (psu). The sound speed profile in the sea floor sediments was simulated by a piecewise-constant average compressional wave speed in the range from 1685 to 1710 m/s. Inversion was performed for the dimensionless parameter s ranging from 1 to 10 on a grid containing 64 nodes. Figure 6.7 shows the results of inversion from the surface of the water column. Although the proposed algorithm performed nicely for the water column, it did not allow for obtaining the fine structure of sediments. The results of inversion from the sea floor are shown in Figure 6.8. In this case, the refinement was resulted in a good reconstructed image, though the accuracy of reconstruction was diminished as we advanced into the sediment layer. The influence of perturbations in the data on the accuracy of reconstruction was very similar to the case of electromagnetic frequency sounding.

6.2. The Slichter-Langer-Tikhonov (SLT) inverse model of electrical prospecting. Recovering the subsurface conductivity in a horizontally stratified Earth from the observed surface potential was originated by Slichter [20] and Langer [13]. In [27] Tikhonov established the uniqueness result for their formulation. In [17] the SLT inverse model, as well as the logarithmic derivative of the conductivity function and Hankel transform was used to justify the local strict convexity and smoothness of the residual functional. In this section we apply the proposed algorithm for the SLT inverse problem.

Assume that the upper-half space is filled with a conductive medium, such that $\sigma = \sigma(z) \geq const. > 0$, and there exists a thin layer $(-\varepsilon, 0), \varepsilon > 0$, such that its conductivity is constant and equals to $\sigma(0) = 1$. The lower half-space $z < -\varepsilon$ is supposed to be filled with a dielectric. Introduce the cylindrical coordinates (r, z) and consider a point-like current electrode placed at **the point** $(r_0, z_0) := (0, z_0), z_0 \in (-\varepsilon, 0)$. Because of the cylindrical symmetry, the voltage potential $V(r, z)$ generated by this current satisfies the following conditions.

$$r^{-1}(rV_r)_r + \sigma^{-1}(z)(\sigma(z)V_z)_z = -\delta(r)\,\delta(z - z_0), r > 0, z > -\varepsilon, \tag{6.19}$$

$$\sigma(0)V_z(r, -\varepsilon) = 0, \tag{6.20}$$

$$\lim_{|(r,z)|\to\infty} V(r, z) = 0. \tag{6.21}$$

We formulate the following inverse problem.

Inverse Problem of Electrical Prospecting. *Let the function $V(r, z)$ satisfies the boundary value problem (6.19)-(6.21) and it is associated with the conductivity $\sigma(z)$. However, the trace $V(r, 0)$ of $V(r, z)$ on the surface $z = 0$ is unknown. Instead, its approximation $\Psi(r)$, such that $\|V(r, 0) - \Psi(r)\| \leq \delta$, is known. Given $(\Psi(r), \delta, \sigma_0, L)$, find an approximation of $\sigma(z)$ in the finite layer $(0, L)$.*

Following [27], we first apply the zero-order Hankel (Fourier-Bessel) transform

$$\tilde{V}(z,\zeta) = \int_0^\infty V(r,z) J_0(\zeta r) r dr,$$

to the problem (6.19)-(6.21) and introduce the new variables

$$t(z) = \int_{z_0}^{z} \sigma^{-1}(\xi) d\xi, \tag{6.22}$$

$x = t/T, s = \sigma(L)\zeta T, n(x) = \sigma(z(xT))/\sigma(L)$, where $a(t) = \sigma(z(t))$ and

$$T = \int_{z_0}^{L} \sigma^{-1}(\xi) d\xi.$$

Then, the problem (6.19)-(6.21) is reduced to the two-point problem

$$u_{xx}(x,s) - s^2 n^2(x) u(x,s) = 0, \quad x \in (0,1), \quad s \in [\underline{s}, \overline{s}], \tag{6.23}$$

$$u_x(0,s) = -\delta(x - x_0), \tag{6.24}$$

$$u_x(1,s) + s u(1,s) = 0. \tag{6.25}$$

Here, $u(x,s) = \tilde{V}(z(xT), s/\sigma(L)T)$. We notice the similarity of this problem with the problem (6.4)-(6.6) modelling frequency sounding of layered media. The only difference is the surface boundary conditions (6.24), which is due to the presence of the current electrode. This observation motivates the following reformulation of the inverse problem.

Let the function $u(x,s)$ be a solution of the problem (6.23)-(6.25) that corresponds to $n(x)$, but $u(0,s)$ is unknown. Instead, an approximation $\varphi(s)$, such that $\|u(0,s) - \varphi(s)\| \leq \delta_\varphi$, where $\delta_\varphi > 0$ and $\varphi(s) = \psi(s/\sigma(L)T)$

$$\psi(\tau) = \int_0^\infty \Psi(r) J_0(\tau r) r dr$$

is given, find an approximation of $n(x)$ in $(0,1)$.

Since the SLT model (6.23)-(6.25) is similar to the frequency sounding model (6.4)-(6.6), the specific procedure for reconstructing the conductivity is the same as described in the section 6.1. However, since the travel time transformation (6.22) maps a uniform grid $\{z_i\}_{i=0}^n$ onto a non-uniform grid $\{t_i\}_{i=0}^n$, such that

$$t_i = \sigma^{-1}(z_i)h + t_{i-1}, \quad t_0 = 0, \quad t_n = T,$$

one needs to transform the reconstructed refraction coefficient back to the conductivity distribution. Let $\tilde{n}_i$ be the values of the reconstructed refraction coefficient on an arbitrary uniform grid $\{\hat{x}_i\}_{i=0}^n$. Then, to obtain the values $\tilde{\sigma}$ of the reconstructed conductivity on $\{z_i\}_{i=0}^n$, we interpolated the values $\tilde{n}_i\sigma(L)$ from the uniform grid $\{\hat{x}_i\}_{i=0}^n$ onto the non-uniform grid $\{t_i/T\}_{i=0}^n$ corresponding to the uniform grid $\{z_i\}_{i=0}^n$. In this case, the "optimal" dimensionless range of the parameter s, i.e., $[\underline{s}, \overline{s}]$, was chosen as $[0.01, 0.1]$.

In case of the SLT model of electrical prospecting the refinement procedure did not lead to the significant improvement of $\sigma_{k_{stop}}(z)$. Therefore, Figures 6.9 and 6.10 show the results of reconstructions without refinement.

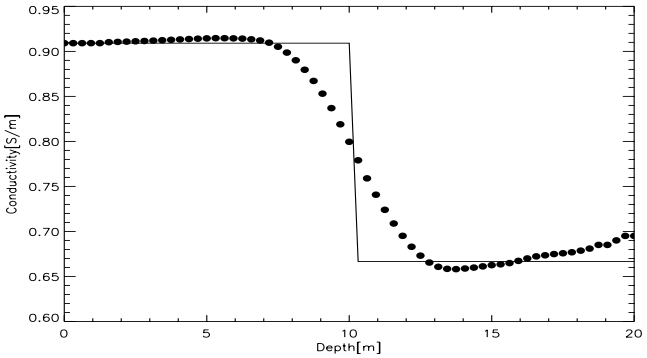

FIG. 6.9. *Inversion of the surface voltage potential (bullets). The original distribution of conductivity for the two-layer medium is shown by the solid line.*

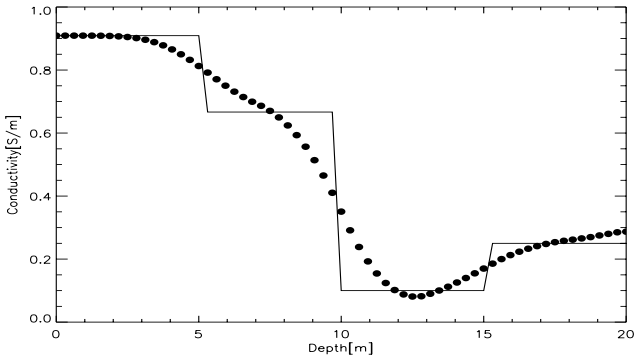

FIG. 6.10. *Inversion of the surface voltage potential (bullets). The original distribution of conductivity for the four-layer medium is shown by the solid line.*

7. Conclusions. We developed a globally convergent algorithm for quantitative imaging in frequency sounding and electrical prospecting of layered media. The convergence of the algorithm was justified. Compared to the existing globally convergent algorithms, the proposed one possesses two new features. These are the iterative procedure for the numerical solution of an overdetrmined boundary value problem for the second-order nonlinear differential equation and the procedure of refinement of an approximate solution. It was demonstrated in the numerical experiments that these novelties may improve, sometimes significantly, both the spatial and contrast resolution of imaging.

Acknowledgment

This work was supported by the U.S. Army Research Laboratory and U.S. Army Research Office under the grant number W911NF-11-1-0399.

REFERENCES

[1] L. BEILINA, *Adaptive finite element/difference method for inverse elastic scattering waves,* Appl. and Comput. Math., **1** (2002), pp. 158-174.

[2] L. BEILINA AND M. V. KLIBANOV, *A globally convergent numerical method for a coefficient inverse problem*, SIAM J. Sci. Comp., **31**(1) 2008, pp. 478–509.

[3] L. Beilina and M. V. Klibanov, *Approximate Global Convergence and Adaptivity for Coefficient Inverse Problems*, Springer-Verlag, NY, 2012.
[4] L. Cagniard, *Basic theory of the nagnetotelluric method of geophysical prospecting*, Geophysics, **37** (1953), pp. 605–635.
[5] Y. Chen and V. Rokhlin, *On the inverse scattering problem for Helmholtz equation in one dimension*, Inverse Problem, **8** (1982), pp. 365–391
[6] K. Key, *Marine electromagnetic studies of seafloor resources and tectonics*, Surveys in Geophysics, **33**(1) (2012), pp. 135–167.
[7] M. V. Klibanov and A. Timonov, *Carleman Estimates for Coefficient Inverse Problems and Numerical Applications*, VSP, Utrecht, 2004.
[8] M. V. Klibanov, A. B. Bakushinsky, and L. Beilina, *Why a minimizer of the Tikhonov functional is closer to the exact solution than the first guess*, J. Inv. Ill-Posed Problems, **19** (2011), pp. 83–105.
[9] E. Ya. Khruslov and D. G. Shepelsky, *Inverse scattering method in electromagnetic sounding theory*, Inverse Problems, **10** (1994), pp. 1–37. pp.507–522
[10] A. V. Kuzhuget and M. V. Klibanov, *Global convergence for a 1-D inverse problem with application to imaging of land mines, Applicable Analysis*, **89** (2010), pp. 125-157.
[11] A. V. Kuzhuget, L. Beilina and M. V. Klibanov, *Approximate global ocnvergence and quasireversibility for a coefficient inverse problem with backscattering data*, J. of Math. Sci., **181** (2012), pp. 19-49.
[12] A. V. Kuzhuget, L. Beilina, M. V. Klibanov et al., *Blind experimental data collected in the field and an approximately globally convergent inverse algorithm*, Inverse Probl., **28**(9) (2012), p. 095007.
[13] R. E. Langer, *On the determination of Earth conductivity from observed surface potentials*, Bul. AMS, **42** (1936), pp. 747–754.
[14] R. Lattes and J. L. Lions *The Method of Quasi-Reversibility: Applications to Partial Differential Equations*, NY, 1969.
[15] M. M. Lavrentiev, V. G. Romanov, and S. P. Shishatskii, *Ill-Posed Problems of Mathematical Physics and Analysis*, AMS Providence, R.I., 1986.
[16] S.LeFounteun, O. Diat, A. Guillermo, at al., *NMR 1D-imaging of water infiltration into mesoporous matrices*, Magn. Reson, Imaging, **29**(3) 2011, pp. 443–455.
[17] B. Mukanova, *An inverse resistivity problem: 2. Unilateral convexity of the objective functional*, Applic. Anal., **88**(5) (2009), pp. 767–788.
[18] S. D. Rajan, G. V. Anand and P. V. Nagesh, *Joint estimation of water column and sediment acoustic properties from broadband towed array data using modal inverse method*, J. Acoust. Soc. Am., **120**(3) (2006), pp. 1324–1334.
[19] A. A. Samarskii, *The Theory of Difference Schemes*, Marcel Dekker, Inc., NY, 2001.
[20] L. B. Slichter, *The interpretation of the resistivity prospecting method for horizontal structures*, Physics, **4** (1933), pp. 307–311.
[21] V. Spichak, *Electromagnetic Sounding of the Earth's Interior*, Elsevier Science, 2011.
[22] M. E. Stewart, N. H. Mack, V. Malyarchuk et al., *Quantitative multispectral biosensing and 1D imaging using quasi-3D plasmonic crystals*, Proc. Natl. Acad. Sci. USA, **103**(46) (2009), pp. 17145–17148.
[23] J. Sylvester, *Layer stripping*, in "Surveys on Solution Methods for Inverse Problems, ed. D. Colton et al., Springer-Verlag, NY, 2000.
[24] A. Tamasan and A. Timonov, *On a new approach to frequency sounding of layered media*, Num. Func. Analysis and Optimization, **29** (3-4) (2008), pp.470–486.
[25] V. P. Tanana, *Methods for Solving the Operator Equations*, Elsevier, NY, 2001.
[26] A. N. Tikhonov, *Mathematical basis of the theory of electromagnetic sounding*, U.S.S.R Comput. Math. Mathem. Phys., **5** (1949), pp. 797–800.
[27] A. N. Tikhonov, *On the uniqueness of the solution to the problem of electrical prospecting*, Doklady U.S.S.R, **LXIX**(6) (1965), pp. 207–211.
[28] A. N. Tikhonov and A. A. Samarskii, *Equations of Mathematical Physics*, Dover, NY, 1963.
[29] A. N. Tikhonov, A. A. Leonov, and A. G. Yagola, *Nonlinear Ill-Posed Problems*, Elsevier, NY, 2001.
[30] M. S. Zhdanov and G. V. Keller, *The Geolectrical Methods in Geophysical Exploration*, Elsevier, NY, 1994.
[31] W. D. Wilson, *Equation for the speed of sound in sea water*, J. Acoust. Soc. Am., **32**(10) (1960), pp. 1357–1373.
[32] *www.asiinstr.comtechnicalDielectric%20Constants.htm*